4D-Flow MRI of aortic and valvular disease

Juffermans, J.F.

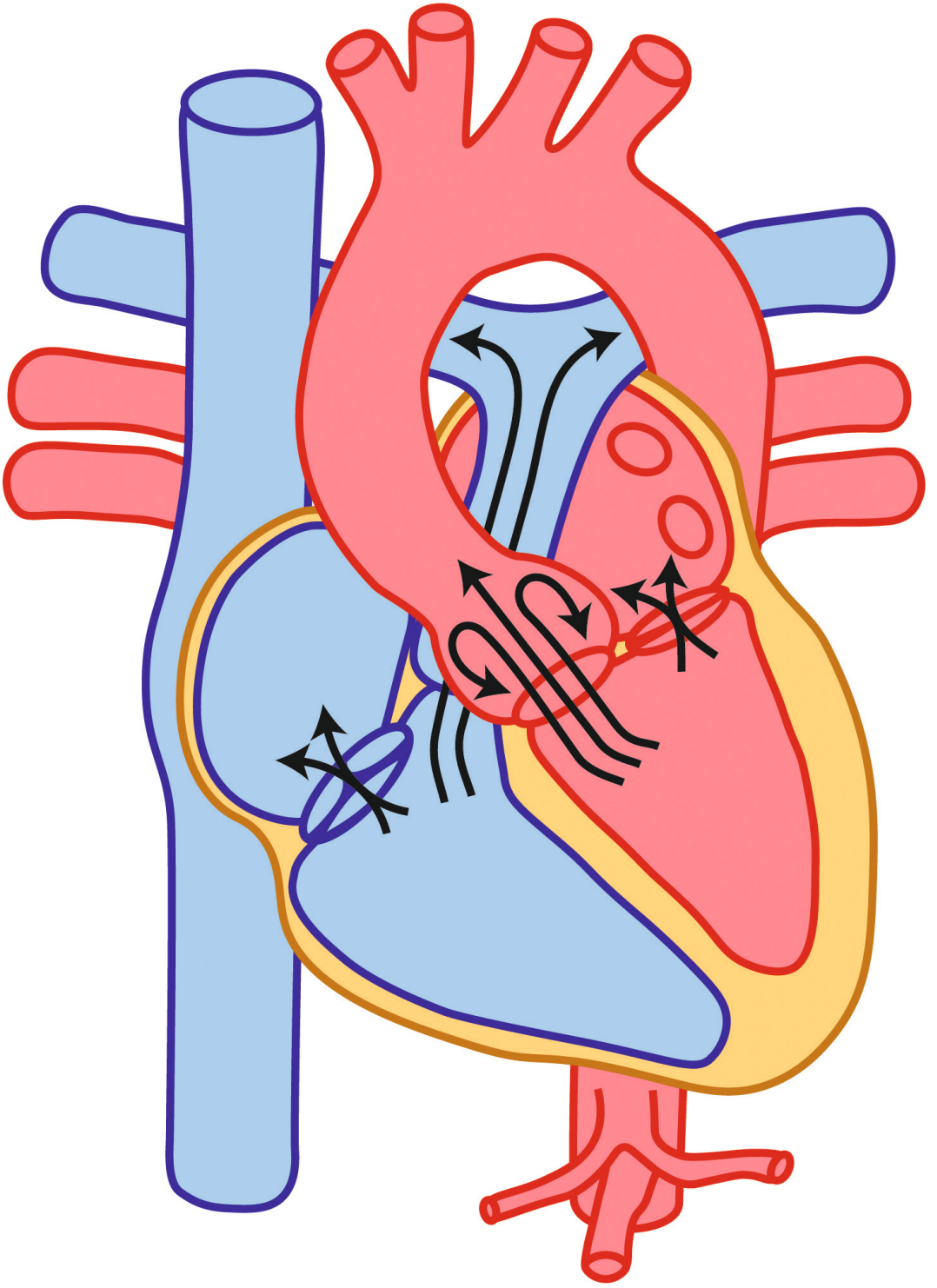

CHAPTER 4

Multicenter Consistency Assessment of Valvular Flow Quantification With Automated Valve Tracking in 4D Flow CMR

Joe F. Juffermans, Savine C. S. Minderhoud, Johan Wittgren, Anton Kilburg, Amir Ese, Benjamin Fidock, Yu-Cong Zheng, Jun-Mei Zhang, Carmen P.S. Blanken, Hildo J. Lamb, Jelle J. Goeman, Marcus Carlsson, Shihua Zhao, R. Nils Planken, Pim van Ooij, Liang Zhong, Xiuyu Chen, Pankaj Garg, Tilman Emrich, Alexander Hirsch, Johannes Töger, and Jos J. M. Westenberg.

JOURNAL OF THE AMERICAN COLLEGE OF CARDIOLOGY: CARDIOVASCULAR IMAGING, 2021, 14.7: 1354-1366.

ABSTRACT

OBJECTIVES. This study determined: 1) the interobserver agreement; 2) valvular flow variation; and 3) which variables independently predicted the variation of valvular flow quantification from 4-dimensional (4D) flow cardiac magnetic resonance (CMR) with automated retrospective valve tracking at multiple sites.

BACKGROUND. Automated retrospective valve tracking in 4D flow CMR allows consistent assessment of valvular flow through all intracardiac valves. However, due to the variance of CMR scanners and protocols, it remains uncertain if the published consistency holds for other clinical centers.

METHODS. Seven sites each retrospectively or prospectively selected 20 subjects who underwent whole heart 4D flow CMR (64 patients and 76 healthy volunteers; aged 32 years [range 24 to 48 years], 47% men, from 2014 to 2020), which was acquired with locally used CMR scanners (scanners from 3 vendors; 2 1.5-T and 5 3-T scanners) and protocols. Automated retrospective valve tracking was locally performed at each site to quantify the valvular flow and repeated by 1 central site. Interobserver agreement was evaluated with intraclass correlation coefficients (ICCs). Net forward volume (NFV) consistency among the valves was evaluated by calculating the intervalvular variation. Multiple regression analysis was performed to assess the predicting effect of local CMR scanners and protocols on the intervalvular inconsistency.

RESULTS. The interobserver analysis demonstrated strong-to-excellent agreement for NFV (ICC: 0.85 to 0.96) and moderate-to-excellent agreement for regurgitation fraction (ICC: 0.53 to 0.97) for all sites and valves. In addition, all observers established a low intervalvular variation (≤10.5%) in their analysis. The availability of 2 cine images per valve for valve tracking compared with 1 cine image predicted a decreasing variation in NFV among the 4 valves (beta = -1.3; p = 0.01).

CONCLUSIONS. Independently of locally used CMR scanners and protocols, valvular flow quantification can be performed consistently with automated retrospective valve tracking in 4D flow CMR.

INTRODUCTION

The evaluation, management, and procedural guidance of patients with valvular heart diseases rely on accurate and consistent quantification of valvular flow [1-3]. Although Doppler echocardiography is the primary imaging modality for assessing valvular flow and presence of regurgitation jets [4, 5], complementary cardiac magnetic resonance (CMR) imaging is used to quantitatively assess valvular flow and regurgitation severity [3, 6].

From a single intracardiac 4-dimensional (4D) flow CMR acquisition, valvular flow and regurgitation jets through all 4 valves can be quantified with retrospective valve tracking [6, 7]. To allow this tracking method, 1 or 2 (orthogonally oriented) complementary valvular cine acquisitions of the valve motion are acquired per valve. In contrast to multiple 2D flow CMR, retrospective valve tracking allows quantification of eccentric regurgitation jets and correction of annular valve plane motion [7-11]. Furthermore, retrospective valve tracking has also demonstrated a superior accuracy with a lower variation in net forward flow assessment among the cardiac valves (i.e., intervalvular variation) [8-15]. To support clinical applicability, retrospective valve tracking was automated recently, which reduced analysis time and improved intervalvular consistency [8].

Because of the international variation of locally used CMR scanners and protocols, it remains uncertain whether previously published reproducibility and consistency results hold for other clinical centers [16]. In addition, the effect of local protocols, such as the CMR scanner vendor, magnetic field strength, contrast agent usage, maximal regurgitation fraction among all valves, and availability of 1 or 2 valvular cine images per valve for valve tracking, on the intervalvular variation is not fully known [16].

We hypothesized that valvular flow quantification with automated retrospective valve tracking in 4D flow CMR resulted in consistent net forward volume (NFV) assessment among the 4 valves at multiple centers, despite differences in locally used CMR scanners and protocols. Subsequently, we hypothesized that the intervalvular variation of NFV was not affected by using a specific CMR scanner vendor, magnetic field strength, or the maximal regurgitation fraction among the valves, but was predicted by the use of contrast agent and availability of 1 or 2 cine images per valve for the valve tracking procedure. Furthermore, we hypothesized that observers agreed upon valvular flow quantification.

Therefore, the purpose of this multicenter study was to determine: 1) the interobserver agreement; 2) valvular flow variation; and 3) variables that independently predicted the variation of valvular flow quantification from 4D flow CMR with automated retrospective valve tracking at multiple sites.

MATERIALS AND METHODS

STUDY POPULATION

Seven clinical centers each retrospectively or prospectively selected 20 datasets of patients, healthy volunteers, or a combination of both (Table 1). Ethical approval and written informed consent were locally obtained for all sites and subjects, respectively. To allow consistency analysis of valvular flow among all 4 heart valves, subjects with intra- and extra-cardiac shunts, or with congenital heart diseases of great complexity (as defined by the American Heart Association) were excluded [17]. From the entire study population, 28 healthy volunteers (20%; included by 2 centers) were reported in earlier studies that described hemodynamic forces and kinetic energy in the ventricles [18-20].

CMR ACQUISTION

All subjects were scanned with locally used clinical CMR scanners and protocols (Table 2). The sites scanned with 3 different CMR vendors and 2 different field strengths (3 Philips Healthcare [Best, the Netherlands], 2 GE Healthcare [Milwaukee, Wisconsin], and 2 Siemens Healthcare [Erlangen, Germany] scanners; 2 1.5-T and 5 3-T scanners). The CMR examination consisted of a whole heart 4D flow CMR protocol covering all intracardiac valves and multiple 2D steady-state, free-precession cine acquisitions to capture the motion of the valves. Depending on the local protocol, each intracardiac valve was imaged with 1 or 2 (orthogonally orientated) cine views (e.g., 2-, 3-, 4-chamber, or outflow tract views).

IMAGE ANALYSIS

Automated retrospective valve tracking was performed over the tricuspid, pulmonary, mitral, and aortic valves using the commercially available CAAS MR Solutions v5.1 software (Pie Medical Imaging, Maastricht, the Netherlands). For each valve, the tracking was manually initiated for each valve by placing 2 annular points per cine view (Central Illustration). Sequential 4D flow CMR-derived, through-valve velocity maps were projected on the cine views to allow misalignment correction between the 4D flow CMR and the cine views. Furthermore, if regurgitation was present, a measurement plane was manually placed in the center of the jet and subsequently automatically angulated perpendicular to the jet direction 0.5 to 1.5 cm proximal to the regurgitant orifice. Next, a time-resolved plane was reconstructed and mapped to the 4D flow CMR to create transvalvular velocity maps with valve contours. The initial automatically generated annulus contours were manually adjusted on the transvalvular velocity maps. Aliasing correction, static tissue offset correction, and valve through-plane motion correction were performed using available algorithms within the image analysis software as described in more detail by Kamphuis et al. [8].

For each of the 4 valves, the software determined the forward volume ($Vol_{Forward}$), backward volume ($Vol_{Backward}$), NFV ($Vol_{Forward} - Vol_{Backward}$), and regurgitation fraction (RF) ($Vol_{Backward}/Vol_{Forward}$). The intervalvular variation in NFV among the 4 valves was calculated per subject by dividing the SD of the NFV of the 4 valves over the mean NFV of the 4 valves.

INTEROBSERVER AGREEMENT

The 20 subjects per center were analyzed at the center of collection by local site observers (S.C.S.M., J.W., A.K., A.E., B.F., Y.Z., J.Z., and C.P.S.B.). To assess the interobserver agreement, the image analysis of all 140 subjects was repeated by 1 central observer (J.F.J.). The local site observers and central observer were supervised by local experienced cardiovascular CMR researchers (A.H., J.T., T.E., P.G., X.C., S.Z., L.Z, P.O., and J.J.M.W.; all with >10 years experience in 4D flow CMR) who verified the image processing. To prevent bias towards their own data, the central site did not contribute data to this study (Leiden University Medical Center, Leiden, the Netherlands). The interobserver variation in NFV was calculated per subject by dividing the mean absolute difference of NFV among all valves by the mean NFV among all valves analyzed by both observers.

To get acquainted with the software, all observers received initial software training by the vendor and studied the standard operator procedure document. Furthermore, all local site observers gained feedback by the central site on 3 randomly selected cases after finishing the image analysis of the first 10 subjects. Thereafter, the local observers reviewed their initial analyses, and, when needed, repeated analysis for the 10 cases and finalized the analysis of all 20 subjects.

STATISTICAL ANALYSIS

Statistical analysis was performed using SPSS v23 software (IBM, Armonk, New York). Continuous parameters are expressed as mean ± SD or as median with lower and upper quartiles (median [Q1 to Q3]). To assess the interobserver agreement of the $Vol_{Forward}$, $Vol_{Backward}$, NFV, and RF per site and per heart valve, Bland-Altman analysis [21], coefficient of variation (COV), intraclass correlation coefficient (ICC), and Pearson's correlation coefficient were calculated. For the Bland-Altman analysis, the mean difference and limits of agreement (±1.96 · SD) were computed by subtracting the central observers' results from local site observers' results. To assess the consistency of NFV among the 4 valves per subject and between observers, the intervalvular and interobserver variations were calculated, respectively. This interobserver agreement and NFV consistency analysis was also conducted for 3 cohorts with different valvular dysfunctions: healthy volunteers only, patients only, and all subjects with a RF ≥15% (scored by the local and central observer) [8]. To assess the predictive value of the choice of CMR scanner vendor, magnetic field strength, contrast agent usage, maximal regurgitation fraction, and the total number of cine images available for tracking of all valves (either 1 or 2 per valve) on the central observer's intervalvular variation, multiple regression analysis was performed with backward elimination (iteratively removing the factor with the highest p

value, until the remaining factors were all significant with p values <0.05). In addition, the regurgitation classification agreement between the 4D flow CMR and echocardiography was assessed retrospectively for all patients if clinical echocardiography was available. The comparison between the regurgitation classification based on 4D flow CMR and echocardiography is presented in the Appendix. The COV and intervalvular and interobserver variation were classified as: low (≤10%); intermediate (11% to 20%); high (21% to 30%); and very high (>30%). The Pearson and ICC coefficients were classified as: poor (<0.50); moderate (0.50 to 0.69); good (0.70 to 0.84); strong (0.85 to 0.94); and excellent (≥0.95). A p value <0.05 was considered statistically significant.

Central Illustration. Despite differences in (A) locally used cardiac magnetic resonance (CMR) imaging scanners and protocols, this study showed that (B) valvular flow quantification with automated retrospective valve tracking of 4-dimensional (4D) flow CMR had (C) a good interobserver agreement and (D) was consistent at multiple centers. (B) Schematic overview of the image analysis steps of retrospective valve tracking, with examples of the mitral and tricuspid valve (upper and lower rows, respectively). The mitral and tricuspid valve are displayed during diastole and systole, respectively. (Step 1) Automated valve tracking of the annular plane in 4-chamber (upper) and 2-chamber (lower) cine views. (Step 2) Inspection of cine views with projected 4D flow CMR-derived through-valve velocity maps. Forward and backward flow are displayed as red and blue, respectively. Because a regurgitation jet present at the tricuspid valve (right), an alternative measurement plane is placed (purple line) on the regurgitant jet, and automatically perpendicularly angulated to the jet direction. (Step 3) Manual delineation of the valve (upper) and regurgitation jet (lower) contours on the transvalvular velocity maps. Forward and backward flow are indicated with a blue and purple line, respectively. (Step 4) Streamline visualization of the 4D flow CMR-derived transvalvular velocity. Mitral inflow and tricuspid regurgitant flow are displayed with red and blue, respectively. (C) Pearson's correlation results of the interobserver agreement. The coefficients of sites and valves are expressed as a range over all sites and valves, respectively. All Pearson's correlations had a p value <0.001. (D) The intervalvular variation of the central observer per site, expressed as median with lower and upper quartiles. The intervalvular variation is the net forward volume SD divided by the mean net forward volume between all 4 valves. LA = left atrium; LV = left ventricle; RA = right atrium; RV = right ventricle.

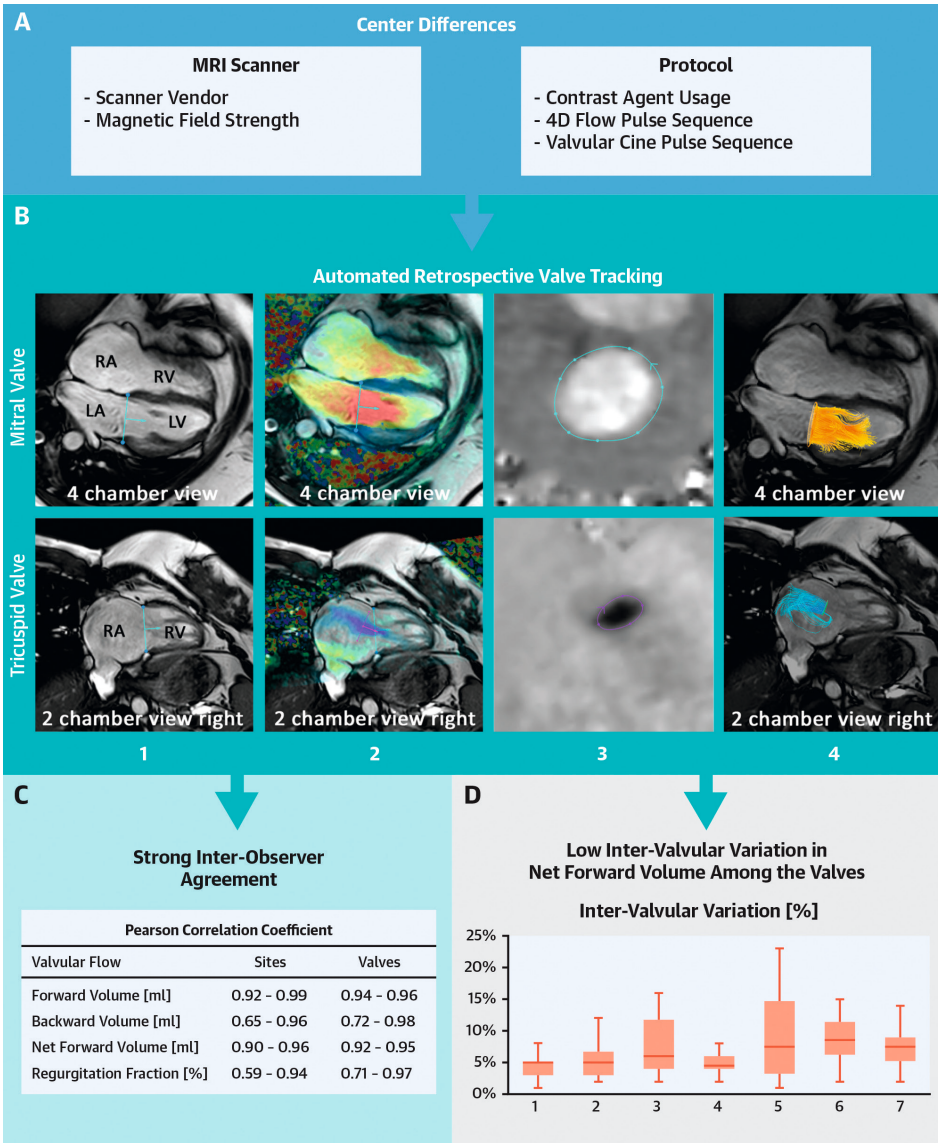

Pearson Correlation Coefficient		
Valvular Flow	Sites	Valves
Forward Volume [ml]	0.92 - 0.99	0.94 - 0.96
Backward Volume [ml]	0.65 - 0.96	0.72 - 0.98
Net Forward Volume [ml]	0.90 - 0.96	0.92 - 0.95
Regurgitation Fraction [%]	0.59 - 0.94	0.71 - 0.97

RESULTS

POPULATION CHARACTERISTICS

Seven clinical centers contributed data to this study with 20 cases per site; this included 64 patients and 76 healthy volunteers (n = 140; age 32 years [range 24 to 48 years]; 47% (66 of 140 subjects) men, from 2014 to 2020). Among the 64 patients, 28 had acquired heart disease and 36 had congenital heart disease. The study population was included retrospectively or prospectively in 62% (87 of 140) and 38% (53 of 140) of all subjects, respectively (from retrospectively selected subjects, 31% [27 of 87] were patients, from prospectively selected subjects, 70% [37 of 53] were patients). Extravascular contrast agents were used in 40% (56 of 140) of all subjects (33% [25 of 76] in healthy volunteers, 48% [31 of 64] in patients).

Retrospective valve tracking was performed on the tricuspid valve, pulmonary valve, mitral valve, and aortic valve using 1 cine image per valve in 21% (29 of 140), 16% (23 of 140), 1% (1 of 140), and 16% (22 of 140) of all subjects, respectively. The valve motion of the remaining 87% (485 of 560) of valves was tracked on 2 cine images per valve. The total number of cine images available for valve tracking was 5 in 4% (5 of 140), 6 in 11% (15 of 140), 7 in 20% (28 of 140), and 8 in 66% (92 of 140) of all subjects. The population characteristics and CMR acquisition details per site are tabulated in Tables 1 and 2, respectively.

INTEROBSERVER AGREEMENT

The results of the interobserver analysis per site and per valve are presented in Tables 3 and 4 and Figures 1 and 2, respectively. In general, for all centers and heart valves, the analysis demonstrated for $Vol_{Forward}$ and NFV a strong-to-excellent Pearson correlation and ICC with a low-to-intermediate COV ($Vol_{Forward}$: r = 0.92 to 0.99; ICC = 0.84 to 0.99; COV = 4.1% to 12.4%; and NFV: r = 0.90 to 0.96; ICC = 0.85 to 0.96; COV = 6.2% to 13.3%). Mean differences in $Vol_{Forward}$ and NFV were ≤5.4 and ≤4.6 ml, respectively, except for 1 site that showed a higher mean difference ($Vol_{Forward}$: 9.7 ml; NFV: 7.6 ml). For $Vol_{Backward}$ and RF, the analysis demonstrated a moderate-to-excellent Pearson's correlation and ICC ($Vol_{Backward}$: r = 0.65 to 0.98; ICC = 0.53 to 0.98; and RF: r = 0.59 to 0.97; ICC = 0.39 to 0.97). Mean differences in $Vol_{Backward}$ and RF were ≤2.2 ml and ≤2.3%, respectively.

Table 1. Study and population characteristics per site.

Site	1	2	3	4	5	6	7
Data Collection							
Range of study [year–year]	2019–2020	2019–2020	2016 - 2019	2018	2014–2019	2015–2018	2017–2019
Population size [n]	20	20	20	20	20	20	20
Retrospective collected subjects [n]	20 (100)	0 (0)	7 (35)	20 (100)	20 (100)	20 (100)	0 (0)
Prospective collected subjects [n]	0 (0)	20 (100)	13 (65)	0 (0)	0 (0)	0 (0)	20 (100)
Subjects reported in earlier studies [n]	0 (0)	0 (0)	8 (40) [19, 20]	0 (0)	0 (0)	20 (100) [18]	0 (0)
Subject Types							
Patients [n]	17 (85)	20 (100)	7 (35)	0 (0)	10 (50)	0 (0)	10 (50)
Patients with acquired heart diseases [n]	7 (35)	10 (50)	5 (25)	0 (0)	1 (5)	0 (0)	5 (25)
Patients with congenital heart diseases [n]	10 (50)	10 (50)	2 (10)	0 (0)	9 (45)	0 (0)	5 (25)
None-to-mild RF (< 15%)	9 (45)	17 (85)	19 (95)	19 (95)	12 (60)	16 (80)	14 (70)
Mild-to-moderate RF (15%–25%)	4 (20)	0 (0)	1 (5)	1 (5)	2 (10)	4 (20)	2 (10)
Moderate-to-Severe RF (26%–48%)	6 (30)	3 (15)	0 (0)	0 (0)	5 (25)	0 (0)	4 (20)
Severe RF (> 48%)	1 (5)	0 (0)	0 (0)	0 (0)	1 (5)	0 (0)	0 (0)
Subject Characteristics							
Male [n]	8 (40)	11 (55)	11 (55)	8 (40)	11 (55)	13 (65)	4 (20)
Age [years]	34 [20–42]	49 [33–60]	33 [26–46]	26 [22–29]	30 [23–41]	43 [22–54]	35 [25–48]
Weight [kg]	63 [59–79]	70 [60–79]	76 [72–92]	66 [61–76]	73 [65–80]	71 [64–77]	56 [46–69]
Height [cm]	166 [159–178]	166 [161–170]	177 [174–185]	173 [169–180]	175 [171–187]	170 [161–174]	159 [152–170]
BMI	22 [20–26]	25 [23–27]	24 [23 -28]	23 [21–25]	24 [22–26]	24 [23–27]	21 [19–25]
BSA	1.7 [1.6–1.9]	1.8 [1.6–1.9]	1.9 [1.8–2.1]	1.8 [1.7–1.9]	1.9 [1.8–2.0]	1.8 [1.6–1.9]	1.6 [1.4–1.7]
Heart Rate [bpm]	70 [55–77]	72 [59–76]	61 [53–69]	69 [63–78]	68 [57–72]	60 [56–77]	68 [62–76]
Contrast Usage							
Extravascular contrast agent [n]	0 (0)	14 (70)	7 (35)	20 (100)	15 (75)	0 (0)	0 (0)

Values are n (%) or median with lower and upper quartiles (median [Q1 - Q3]) unless otherwise indicated. Abbreviations: BMI = body mass index; BSA = body surface area; RF = maximal regurgitation fraction scored by the central observer.

Table 2. MRI acquisition details per site.

Site	**1**	**2**	**3**	**4**	**5**	**6**	**7**
Site							
City	Amsterdam	Beijing	Lund	Mainz	Rotterdam	Sheffield	Singapore
Country	The Netherlands	China	Sweden	Germany	The Netherlands	United Kingdom	Singapore
MRI Scanner							
Vendor	Philips Healthcare	GE Healthcare	Siemens Healthineers	Siemens Healthineers	GE Healthcare	Philips Healthcare	Philips Healthcare
Type	Ingenia	Discovery MR 750	MAGNETOM Aera	MAGNETOM Prisma	Patients: Discovery MR450 Volunteer: Signa Artist	Ingenia	Ingenia
Field strength [T]	3	3	1.5	3	1.5	3	3
Total number of available anterior coil elements [n]	24	4	18	18	16	16	16
Total number of available posterior coil elements [n]	8	4	32	32	16	12	12

Table 2. *Continued*

Site	1	2	3	4	5	6	7
4D Flow Pulse Sequence							
Acquired spatial resolution [mm^3]	Patients: 2.5 x 2.5 x 2.5 Volunteer: 3.0 x 3.0 x 3.0	2.0 x 2.0 x 2.4	3.0 x 3.0 x 3.0	2.4 x 3.5 x 3.8	1.7 x 2.1 x 1.8	3.0 x 3.0 x 3.0	3.0 x 3.0 x 3.0
Reconstructed spatial resolution [mm^3]	Patients: 2.4 x 2.4 x 2.5 Volunteer: 2.8 x 2.8 x 3.0	1.4 x 1.4 x 1.2	3.0 x 3.0 x 3.0	2.4 x 2.4 x 3.8	1.4 x 1.4 x 1.3	2.3 x 2.3 x 3.0	1.5 x 1.5 x 1.5
Reconstructed temporal resolution [ms]	29 [26–37]	33 [31–38]	25 [21–29]	44 [38–48]	37 [31–43]	34 [28–36]	29 [26–32]
Reconstructed phases [n]	30	25	40	20	Patients: 20 Volunteers: 30	30	30
Echo time [ms]	1.9	2.1	1.5	2.3	Patients: 1.5 Volunteers: 2.0	3.5	3.7
Repetition time [ms]	3.8	4.3	5.4	4.6	Patients: 3.8 Volunteers: 4.1	10.0	7.5
Flip Angle [degrees]	8	10	With contrast: 15 Without contrast: 8	7	With contrast: 15 Without contrast: 5	10	10
Readout method	Cartesian	Cartesian	Cartesian	Cartesian	Cartesian	Cartesian	Cartesian

Table 2. *Continued*

Site	1	2	3	4	5	6	7
4D Flow Pulse Sequence							
Cardiac gating	Retrospective	Retrospective	Retrospective	Retrospective	Retrospective	Retrospective	Retrospective
Hemi-diaphragm respiratory navigator gating	No	No	No	Yes	No	No	No
Acceleration Method	Pseudo-spiral under sampling with CS-reconstruction [23]	Kat-ARC [24], outer 8, ACS 2	GRAPPA 2x2, Partial Fourier: phase 6/8, slice 6/8	GRAPPA 3x1	Patients: compressed sensing, phase 2, slice 2 [25] Volunteers: Kat-ARC [24], outer 6, ACS 2.	EPI 5, Sense 2	EPI 5, Sense 2
Flow-encoding scheme	Asymmetric four-point	Symmetric four-point	Symmetric four point	Symmetric four point	Symmetric four-point	Asymmetric four-point	Asymmetric four-point
VENC [cm/s]	Acquired: 150 [150–200] Reconstructed: 225 [200–280]	140 [130–150]	Patients: 200 Volunteer: 100	150	Patients: 250 [240–250] Volunteers: 180	150	150
Sequence type	In-house developed [23]	Product	Prototype	Prototype	Patients: Prototype [25] Volunteers: Product	Prototype	Prototype

Table 2. *Continued*

Site	1	2	3	4	5	6	7
Valvular cine pulse sequence							
Total number of valvular cine images over al valves	8	8	7 [5–7]	8	7 [6–8]	7	8
Sequence	SSFP	SSFP	SSFP	SSFP	SSFP	SSFP	SSFP
Acquired spatial resolution [mm^3]	1.6 x 2.0 x 8.0	1.5 x 1.8 x 8.0	1.7 x 1.7 x 6.0	1.7 x 1.3 x 6.0	Patients: 1.5 x 1.6 x 8.0 Volunteers: 1.3 x 1.9 x 6.0	1.9 x 2.0 x 8.0	2.5 x 2.5 x 8.0
Field of View [mm^2]	350 x 350	340 x 340	340 x 340	340 x 340	Patients: 320 x 340 Volunteers: 260 x 360	350 x 350	300 x 300
Reconstructed phases [n]	30	25	25 or 30	25	Patients: 24 Volunteers: 30	30	30
Echo time [ms]	1.4	1.6	1.2	1.4	Patients: 1.3 Volunteers: 1.7	1.5	1.4
Repetition time [ms]	2.8	3.2	2.6	3.2	Patients: 3.0 Volunteers: 3.7	3.0	2.9
Flip Angle [degrees]	45	50	65	52	Patients: 45-60 Volunteers: 65	60	45

Abbreviations: CMR = cardiac magnetic resonance; SSFP = steady-state free-precession; VENC=¼ velocity encoding.

NFV VARIATION

The results of the NFV variation analysis are presented in Table 5 and Figure 3. In general, all observers had a low mean intervalvular variation ≤10.5%; only small differences in intervalvular variation were observed among the sites. For most sites, the mean interobserver variation was ≤5.7%, except for 2 sites that showed a slightly higher but still low variance (7.9% and 8.7%). The multiple regression analysis demonstrated that only the total number of cine images (1 or 2 per valve) that were available for the valve tracking procedure was a significant independent factor (beta = -1.3; p = 0.01) for the central observer's intervalvular variation (Table 6). Therefore, the availability of 2 cine images per valve for valve tracking, compared with 1 cine image, predicted a decreasing intervalvular variation.

VALVULAR DYSFUNCTION

The results of the 3 cohorts are presented in Tables 5 and 7. The cohort of subjects with a RF ≥15% included 30 valves (10 tricuspid, 15 pulmonary, 4 mitral, and 1 aortic valve) from 25 subjects [18%; 25 of 140], 24 patients, and 1 healthy control subject). In general, for all cohorts, the analysis demonstrated a strong-to-excellent Pearson's correlation and ICC with a low COV for all parameters (r = 0.54 to 0.97; ICC = 0.68 to 0.98; and COV = 7.0% to 10.8%). Furthermore, the observers had a low mean intervalvular and interobserver variation (≤6.1% and ≤5.8%, respectively). For the subjects with only RF ≥15%, larger limits of agreements were found for $Vol_{Backward}$ and RF compared with the other cohorts (16.3 ml and 12.7% versus 7.0 to 8.3 ml and 7.7 to 8.4%, respectively). As shown in the Supplemental Appendix, the regurgitation classification based on 4D flow CMR and echocardiography showed a good agreement (weighted kappa = 0.79; p < 0.01 and Spearman rho: r = 0.72; p < 0.01).

Table 3. Interobserver agreement results over all subjects and valves per site.

Parameter	Site	Number of valves	Site Observer	Central Observer	Bland-Altman		Pearson correlation*	ICC	COV [%]
					Diff	LoA			
Forward Volume [mL]	1	80	85.8 [71.4–100.8]	86.3 [72.5–103.5]	-1.4	7.1	0.99	0.99	4.1
	2	80	71.0 [55.9–85.0]	81.4 [63.7–91.0]	-9.7	18.3	0.92	0.84	12.4
	3	80	106.1 [93.7–115.4]	106.4 [93.0–118.9]	-0.3	14.2	0.93	0.93	7.0
	4	80	88.9 [83.0–103.1]	94.3 [85.6–108.2]	-3.7	10.2	0.95	0.93	5.5
	5	80	84.9 [74.5–102.8]	86.6 [75.1–105.7]	-2.5	10.4	0.97	0.96	5.9
	6	80	92.9 [71.0–105.4]	94.4 [74.3–108.5]	-2.6	13.8	0.95	0.95	7.7
	7	80	59.6 [55.1–68.9]	65.0 [57.8–76.7]	-5.4	13.2	0.94	0.89	10.4
Backward Volume [mL]	1	80	3.5 [0.3–10.3]	2.8 [0.2–9.4]	0.3	9.9	0.95	0.95	…
	2	80	0.0 [0.0–0.1]	0.9 [0.1–3.9]	-2.1	6.8	0.88	0.76	…
	3	80	1.7 [0.3–5.5]	1.1 [0.1–3.2]	0.7	5.3	0.75	0.74	…
	4	80	1.1 [0.4–2.4]	1.9 [0.1–4.1]	-1.0	5.4	0.65	0.53	…
	5	80	1.9 [0.6–7.4]	2.3 [0.2–7.0]	0.6	8.5	0.96	0.95	…
	6	80	0.5 [0.1–2.1]	1.0 [0.2–5.7]	-2.2	7.9	0.78	0.47	…
	7	80	2.1 [0.5–5.5]	2.2 [0.1–6.4]	-0.8	6.4	0.96	0.93	…

Table 3. *Continued*

Parameter	Site	Number of valves	Site Observer	Central Observer	Bland-Altman		Pearson correlation*	ICC	COV [%]
					Diff	LoA			
Net Forward Volume [mL]	1	80	76.4 [66.6–91.0]	78.1 [68.8–95.1]	-1.7	9.8	0.96	0.96	6.3
	2	80	70.6 [55.8–82.3]	77.0 [62.2–86.3]	-7.6	19.0	0.90	0.85	13.3
	3	80	101.9 [92.4–112.6]	103.6 [91.8–115.9]	-1.0	13.5	0.93	0.93	6.8
	4	80	87.7 [81.3–101.4]	91.1 [84.6–101.5]	-2.7	11.3	0.93	0.92	6.2
	5	80	78.3 [69.0–93.7]	84.1 [71.2–100.5]	-3.1	13.7	0.92	0.90	8.5
	6	80	91.0 [70.2–104.4]	92.4 [68.9–103.5]	-0.4	14.6	0.94	0.94	8.4
	7	80	56.3 [51.8–63.7]	61.4 [54.3–68.0]	-4.6	12.0	0.93	0.87	10.2
Regurgitation Fraction [%]	1	80	4.5 [0.0–13.8]	3.0 [0.0–11.5]	0.8	8.5	0.94	0.93	–
	2	80	0.0 [0.0–0.0]	1.0 [0.0–5.0]	2.3	7.0	0.83	0.73	–
	3	80	1.0 [0.0–5.0]	1.0 [0.0–3.0]	0.7	4.8	0.74	0.72	–
	4	80	1.0 [0.0–3.0]	2.0 [0.0–4.0]	-1.0	4.9	0.59	0.53	–
	5	80	2.0 [1.0–9.0]	2.0 [0.0–8.0]	0.8	5.1	0.90	0.89	–
	6	80	1.0 [0.0–2.0]	1.0 [0.0–6.0]	-2.0	8.2	0.65	0.39	–
	7	80	4.0 [1.0–8.0]	3.0 [0.0–8.8]	-0.3	6.9	0.94	0.93	–

Values are median with lower and upper quartiles (median [Q1 - Q3]). Net forward volume is the forward volume minus backward volume. RF is the backward volume divided by forward volume. *All Pearson correlations had a p value <0.001. Abbreviations: COV = coefficient of variation; Diff = mean difference; ICC = intraclass correlation coefficient; LoA = limits of agreement (1.96 · SD of difference); RF = maximal regurgitation fraction scored by the central observer.

Table 4. Interobserver agreement results over all subjects per valve.

Parameter	Valve	Number of subjects	Site Observer	Central Observer	Bland-Altman		Pearson correlation*	ICC	COV [%]
					Diff	LoA			
Forward Volume [mL]	Tricuspid	140	86.6 [67.8–108.3]	91.1 [74.1–113.8]	-4.9	15.3	0.95	0.94	8.6
	Pulmonary	140	86.0 [69.2–98.6]	86.5 [71.3–101.0]	-2.5	14.0	0.95	0.95	8.3
	Mitral	140	85.7 [69.4–104.1]	89.8 [72.0–107.9]	-4.1	14.6	0.95	0.93	8.5
	Aorta	140	80.7 [63.6–99.8]	84.0 [67.3–101.9]	-3.0	11.3	0.97	0.96	7.0
Backward Volume [mL]	Tricuspid	140	3.5 [1.2–7.5]	6.3 [2.9–10.4]	-1.8	9.4	0.91	0.90	–
	Pulmonary	140	0.3 [0.0–1.6]	0.2 [0.0–1.7]	0.0	5.7	0.98	0.98	–
	Mitral	140	2.4 [1.0–5.1]	3.1 [1.3–5.7]	-1.0	9.4	0.77	0.72	–
	Aorta	140	0.3 [0.1–1.0]	0.2 [0.0–0.6]	-0.2	3.7	0.87	0.86	–
Net Forward Volume [mL]	Tricuspid	140	80.5 [64.0 -101.5]	84.6 [67.8–102.8]	-3.0	15.1	0.95	0.94	9.2
	Pulmonary	140	77.8 [64.4–95.9]	82.7 [66.7–98.2]	-2.5	13.2	0.95	0.94	8.4
	Mitral	140	80.9 [63.9–101.2]	84.5 [68.2–102.1]	-3.2	16.8	0.93	0.92	10.3
	Aorta	140	79.8 [62.8–98.8]	83.0 [67.2–101.4]	-3.2	11.8	0.96	0.95	7.3
Regurgitation Fraction [%]	Tricuspid	140	5.0 [1.0–9.0]	7.0 [3.0–11.0]	-1.7	9.9	0.83	0.81	–
	Pulmonary	140	0.0 [0.0–2.0]	0.0 [0.0–2.0]	0.3	5.3	0.97	0.97	–
	Mitral	140	3.0 [1.0–6.0]	3.0 [2.0–6.8]	-0.8	9.3	0.72	0.71	–
	Aorta	140	0.0 [0.0–1.0]	0.0 [0.0–1.0]	0.4	4.2	0.78	0.77	–

Values are median with lower and upper quartiles (median [Q1 - Q3]). Net forward volume is the forward volume minus backward volume. RF is the backward volume divided by forward volume. *All Pearson correlations had a p value <0.001. Abbreviations: COV - coefficient of variation, Diff - mean difference, ICC - intra-class correlation coefficient, LoA - limits of agreement (1.96 * standard deviation of difference).

Table 5. Valvular variation results over all subjects per site and per cohort.

Sites	Number of subjects	Inter-valvular variation [%]		Interobserver variation [%]
		Site observer	Central observer	
1	20	4.8 [3.0 – 8.3]	4.5 [2.9 – 5.3]	3.9 [2.6 – 5.1]
2	20	4.2 [1.8 – 5.9]	5.0 [3.0 – 6.5]	7.9 [5.6 – 14.4]
3	20	10.5 [7.7 – 14.3]	5.6 [3.8 – 11.5]	4.0 [3.2 -7.6]
4	20	6.7 [5.0 – 8.3]	4.6 [3.8 – 6.4]	4.0 [2.6 – 5.1]
5	20	5.9 [3.5 – 12.9]	7.6 [3.1 – 14.6]	4.9 [3.5 – 8.7]
6	20	7.5 [3.7 – 9.9]	8.5 [6.4 – 11.2]	5.7 [4.6 – 7.4]
7	20	4.2 [4.0 – 4.8]	7.4 [5.4 – 9.5]	8.7 [4.9 – 12.1]
Cohorts	**Number of subjects**	**Inter-valvular variation [%]**		**Interobserver variation [%]**
		Site observer	**Central observer**	
Healthy controls	76	5.9 [4.0 – 9.4]	6.1 [3.8 – 9.3]	4.7 [3.1 -7.1]
Patients	64	5.3 [3.7 – 8.6]	5.6 [3.6 – 8.3]	5.8 [4.2 – 9.6]
≥15% RF*	25	5.5 [3.7 – 8.5]	4.8 [3.3 – 8.0]	5.2 [3.7 – 9.0]

Values are median with lower and upper quartiles (median [Q1 - Q3]). The intervalvular variation is the net forward volume (NFV) SD divided by the mean net forward volume among all 4 valves. The interobserver variation is the mean absolute difference of NFV among the 4 valves divided by the mean NFV among all valves of both observers. *All subjects with ≥15% Regurgitation Fraction (RF)

TABLE 6 – Multiple regression analysis.

Model	Parameter	Beta	significance
1	MRI scanner vendor	-0.7	.39
	Magnetic field strength	-1.8	.19
	Contrast agent usage	0.6	.64
	Maximal regurgitant fraction among the valve	1.0	.78
	Total number of cine images of all the valves*	-0.9	.18
2	MRI scanner vendor	-0.7	.37
	Magnetic field strength	-1.8	.18
	Contrast agent usage	0.6	.64
	Total number of cine images of all the valves*	-0.9	.17
3	MRI scanner vendor	-0.5	.45
	Magnetic field strength	-1.7	.19
	Total number of cine images of all the valves*	-0.9	.18
4.	Magnetic field strength	-1.2	.29
	Total number of cine images of all the valves*	-1.0	.12
5	Total number of cine images of all the valves*	-1.3	.01

* – the total number of cine images available for valve tracking of all valves (either one or two per valve).

Table 7. Inter-observer agreement results per cohort.

Parameter	Cohort	Number of valves	Site Observer	Central Observer	Bland-Altman		Pearson correlation*	ICC	COV [%]
					Diff	LoA			
Forward Volume [mL]	Healthy controls	304	92.8 [75.6 – 106.9]	95.5 [80.6 – 109.7]	-3.1	12.5	0.95	0.97	7.0
	Patients	256	75.0 [58.9 – 92.9]	78.6 [63.3 – 95.8]	-4.2	15.5	0.95	0.97	10.0
	RF ≥15% **	30	101.9 [83.2 – 125.9]	106.2 [91.4 – 129.3]	-4.8	14.8	0.97	0.98	7.2
Backward Volume [mL]	Healthy controls	304	1.1 [0.3 – 3.4]	1.3 [0.1 – 5.0]	-0.8	7.0	0.58	0.71	...
	Patients	256	1.0 [0.1 – 5.7]	1.6 [0.2 – 5.8]	-0.5	8.3	0.95	0.97	...
	RF ≥15% **	30	27.4 [17.1 – 44.1]	30.3 [18.1 – 47.2]	-2.1	16.3	0.94	0.97	...
Net Forward Volume [mL]	Healthy controls	304	90.7 [72.1 – 103.5]	92.8 [77.5- 105.9]	-2.4	13.2	0.94	0.97	7.5
	Patients	256	70.4 [55.6 – 85.0]	73.5 [59.4 – 86.2]	-3.7	15.4	0.93	0.95	10.8
	RF ≥15% **	30	67.6 [52.5 -83.4]	71.4 [54.8 – 84.8]	-2.7	14.9	0.92	0.91	10.8
Regurgitation Fraction [%]	Healthy controls	304	1.0 [0.0 – 4.0]	1.0 [0.0 – 5.0]	-0.6	7.7	0.54	0.68	...
	Patients	256	1.0 [0.0 – 8.0]	2.0 [0.0 – 8.0]	-0.2	8.4	0.92	0.96	...
	RF ≥15% **	30	28.5 [19.8 – 39.3]	29.0 [18.0 – 40.3]	-0.3	12.7	0.88	0.94	...

Continuous data are reported as median and interquartile range (median [Q_1 - Q_3]). Net forward volume is the forward volume minus backward volume. RF is the backward volume divided by forward volume. *: All Pearson correlations had a p-value smaller than 0.001. **: All valves with regurgitation fraction ≥15%. Abbreviations: COV - coefficient of variation, Diff - mean difference, ICC - intra-class correlation coefficient, LoA - limits of agreement (1.96 * standard deviation of difference).

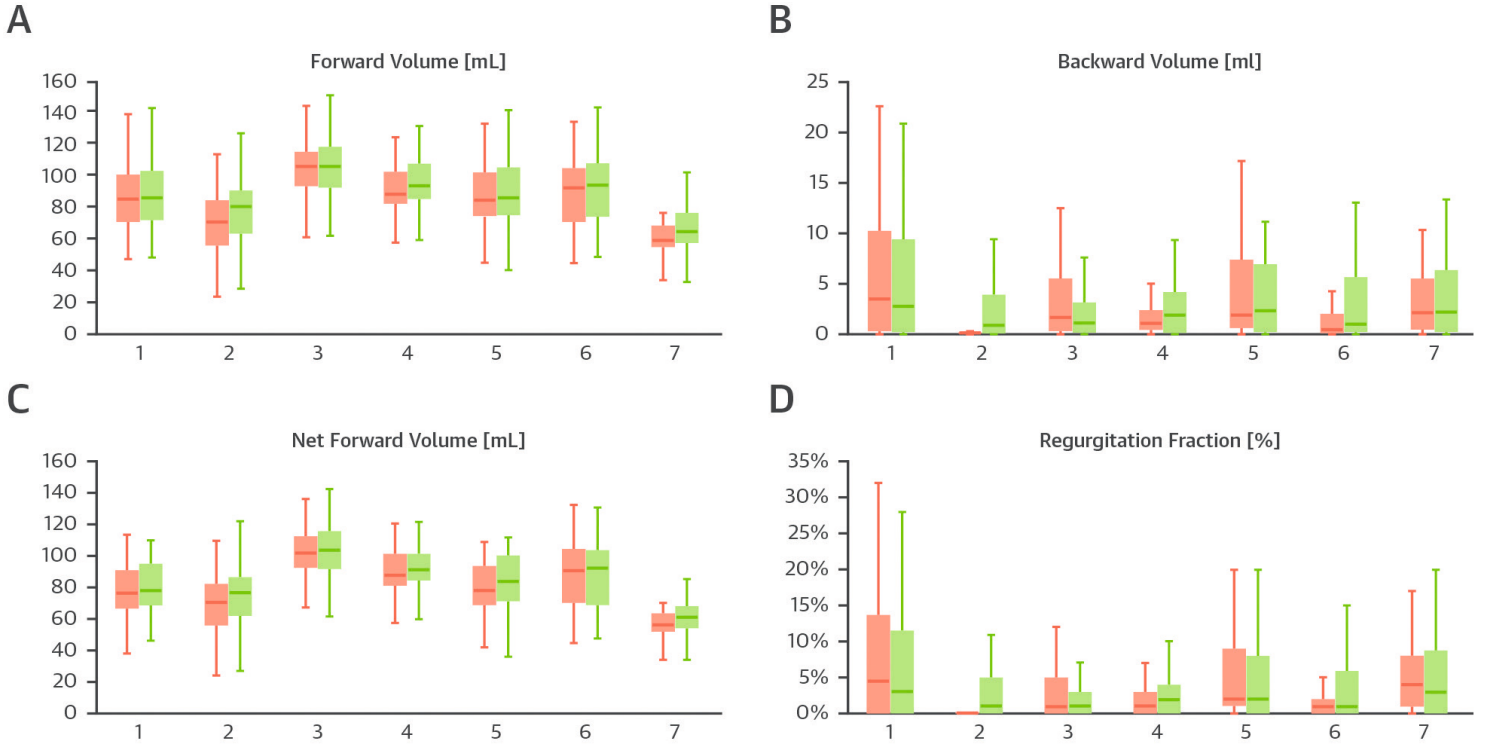

Figure 1. Boxplot of the (A) forward volume, (B) backward volume, (C) net forward volume, and (D) regurgitation fraction among all valves and subjects per site. The results from site observer and central observer are displayed in red and green, respectively.

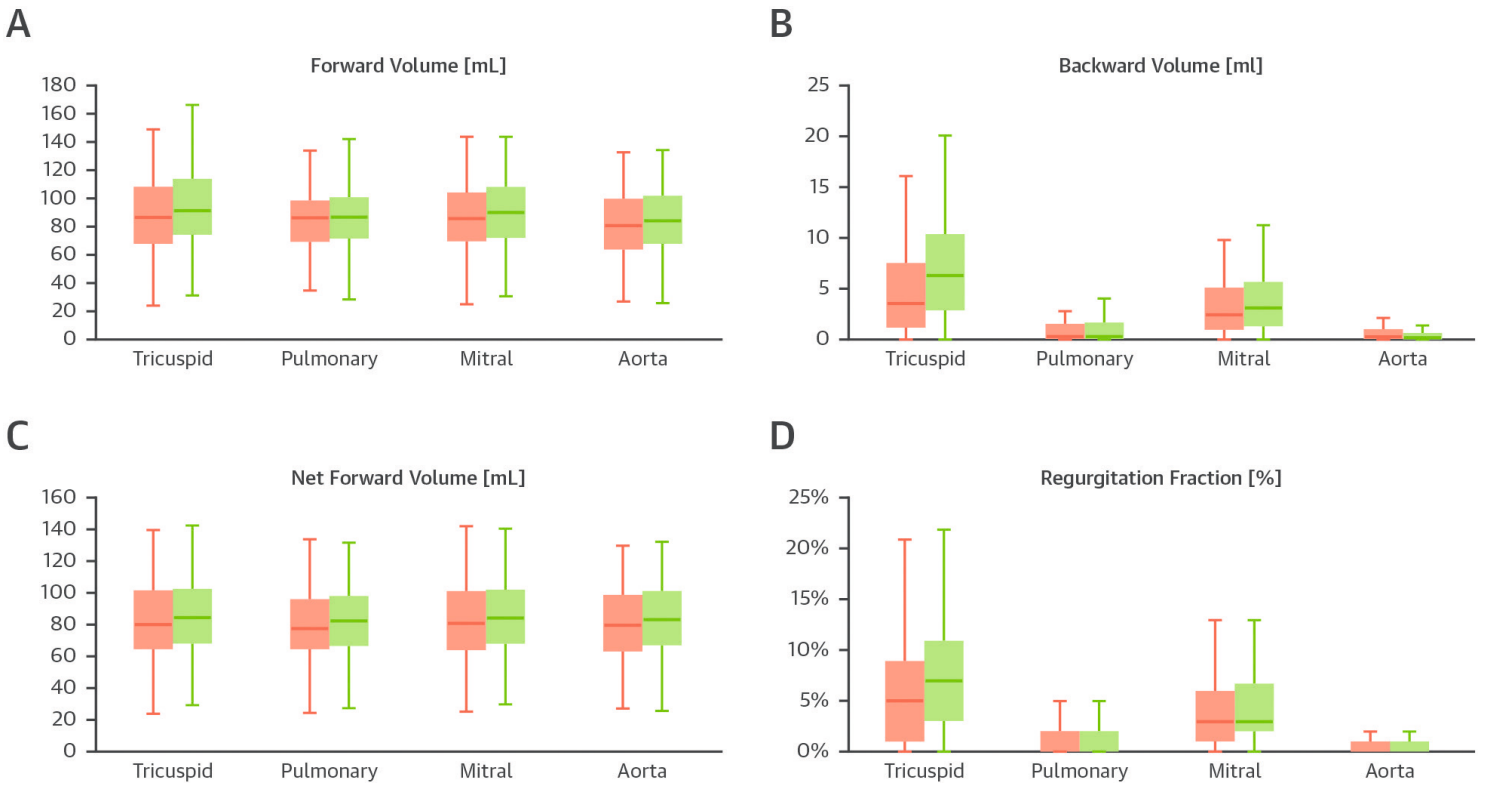

Figure 2. Boxplot of the forward volume (A), backward volume (B), net forward volume (C) and regurgitation fraction (D) among all subjects and sites per valve. The results from site observer and central observer are displayed in red and green, respectively.

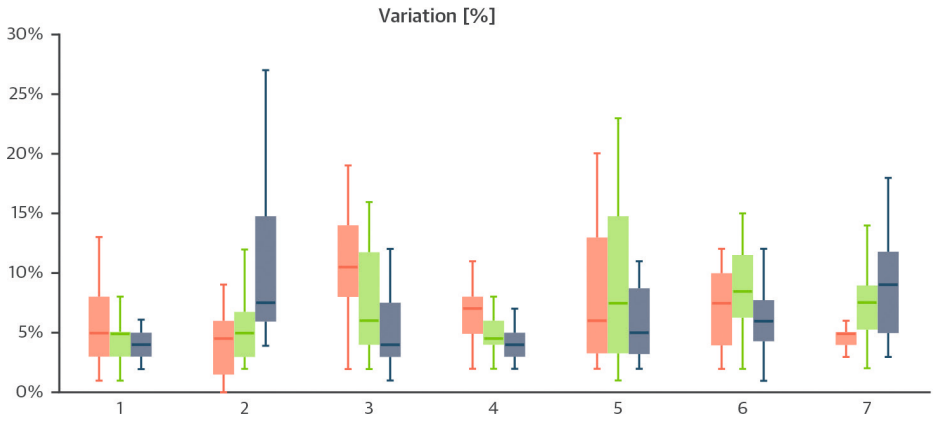

Figure 3. The intervalvular variation of the results from site observers and central observer are displayed in red and green, respectively. The interobserver variation results are displayed in blue. The intervalvular variation was calculated per subject by dividing the SD of the net forward volume (NFV) of the 4 valves over the mean NFV of the 4 valves. The interobserver variation was calculated per subject by dividing the mean absolute difference of NFV among the 4 valves by the mean NFV among all valves of both observers.

DISCUSSION

The purpose of this study was to evaluate consistency in valvular flow quantification using automated retrospective valve tracking in whole heart 4D flow CMR across multiple centers. This was done by determining the interobserver agreement and the NFV variation and evaluating independent predictors that had significant effect on intervalvular variation. The main findings were: 1) the interobserver analysis demonstrated strong-to-excellent agreement for forward volume and NFV and moderate-to-excellent agreement for backward volume and RF for all sites and valves; 2) intervalvular and interobserver variations were low; 3) the number of available cine images per valve for the automated valve tracking procedure was a significant predictor, with 2 images per valve showing lower intervalvular variation among all valves other than 1 valve; and 4) the performance of automated retrospective valve tracking was generally comparable for different degrees of valvular dysfunction.

INTEROBSERVER AGREEMENT.

Patients with valvular heart diseases rely on accurate and consistent quantification of valvular flow and regurgitation jets [1-3]. Although Doppler echocardiography is the primary imaging modality, 4D flow CMR is used complementary to quantitatively assess valvular flow over all 4 valves. For automated retrospective valve tracking in 4D flow CMR, Kamphuis et al. [8] reported a strong-to-excellent interobserver reproducibility for the NFV and RF assessment. In the present study, comparable or slightly lower but still strong interobserver agreement was found among all participating centers and among all cardiac valves. These results demonstrated that the interobserver agreement

of valvular flow assessment was strong and comparable for all cardiac valves with automated retrospective valve tracking.

Furthermore, Kamphuis et al. [8] reported a smaller intervalvular variation for automated retrospective valve tracking for patients and healthy volunteers compared with manual valve tracking. In the present study, comparable intervalvular variation for automated valve tracking was found for approximately one-half of the observers, but the other observers had a slightly higher intervalvular variation. Still, most of the observers analyzed the data with an intervalvular variation well below the reported manual valve tracking variation [8]. Therefore, the results of this study supported the use of automated retrospective valve tracking for reliable valvular flow quantification. The studies that reported manual tracking all used 2 cine views per valve for tracking [8-15], and this was not available in all cases in our study.

NFV VARIATION

A true gold standard for forward flow and regurgitation assessment is lacking [5, 6]; however, a low variation in NFV among the 4 valves, as found in the present study, is consistent with the physiological principle of mass conservation among the 4 valves in absence of a cardiac shunt. Therefore, a low intervalvular variation demonstrated reliable assessment of valvular flow. Moreover, we found that the interobserver variation of NFV was, in general, lower than the intervalvular variation of NFV. This means that the quantitative disagreement between observers was lower than the technical limitations of the 4D flow technique.

Based on the regression analysis outcomes, it is recommended to acquire not 1 but 2 cine views for each heart valve, orthogonally oriented to each other and perpendicular to the annulus, to track the valves accurately and to obtain the lowest intervalvular variation. The availability of 2 cine views decreased the risk of incorrect angulation perpendicular to the view. Furthermore, the use of 2 cine views might simplify and improve the valve tracking, contour delineation, and identification of regurgitation jets. Notably, the use of a contrast agent was not a significant independent predictor, and therefore, did not affect the intervalvular consistency. Because variation in the temporal and spatial resolutions of the 4D flow data among the sites was small and settings on all sites were below or close to the consensus values (i.e., spatial resolution <3.0 × 3.0 × 3.0 mm3 and temporal resolution <40 ms) [16, 22], the predictive value of these parameters was not assessed.

VALVULAR DYSFUNCTION.

The clinical applicability of automated retrospective valve tracking depends on the accuracy and consistency of valvular flow quantifications, especially in patients with relevant valvular dysfunction or regurgitation jets. The analysis demonstrated comparable interobserver agreements and NFV variations among the cohorts.

The subjects with only RF ≥15% demonstrated more variance for $Vol_{Backward}$ and RF. Furthermore, good agreement and correlation was found between 4D flow CMR and echocardiography examinations for regurgitation classification in patients. These results demonstrated that the flow quantification was somewhat less consistent among observers compared with the other cohorts for clinically relevant RF. This decreased interobserver agreement was potentially the result of complicated analysis in the presence of multiple or (time-varying) eccentric regurgitation jets. The performance of the image analysis tool for the specific assessment of these types of valve lesions was beyond the scope of the present study. The low prevalence of severe valve regurgitation in the population might have affected the agreement and correlation assessment of regurgitation classification between the 4D flow CMR and echocardiography examinations.

STUDY LIMITATIONS.

A limitation of the present study was the exclusion of patients with intra- and extracardiac shunts or with congenital heart diseases of great complexity. These patients were excluded to allow consistency analyses based on the intervalvular variation among all 4 cardiac valves. The present study only included adult subjects and no children. Therefore, to advance the present study, future research could be done on the excluded patient populations and on children. Finally, none of the sites used an intravascular contrast agent, which eliminated the possibility to study its effect on the NFV variation.

CONCLUSION

This study showed that, independently of locally used CMR scanners and protocols, valvular flow quantification can be performed consistently with automated retrospective valve tracking in 4D flow CMR.

REFERENCES

1. Nishimura, R.A., et al., 2019 AATS/ACC/ASE/SCAI/STS expert consensus systems of care document: a proposal to optimize care for patients with valvular heart disease: a joint report of the American Association for Thoracic Surgery, American College of Cardiology, American Society of Echocardiography, Society for Cardiovascular Angiography and Interventions, and Society of Thoracic Surgeons. Journal of the American College of Cardiology, 2019. 73(20): p. 2609-2635.
2. Nishimura, R.A., et al., 2017 AHA/ACC focused update of the 2014 AHA/ACC guideline for the management of patients with valvular heart disease: a report of the American College of Cardiology/American Heart Association Task Force on Clinical Practice Guidelines. Journal of the American College of Cardiology, 2017. 70(2): p. 252-289.
3. O'Gara, P.T., et al., 2017 ACC expert consensus decision pathway on the management of mitral regurgitation: a report of the American College of Cardiology Task Force on Expert Consensus Decision Pathways. Journal of the American College of Cardiology, 2017. 70(19): p. 2421-2449.
4. Doherty, J.U., et al., ACC/AATS/AHA/ASE/ASNC/HRS/SCAI/SCCT/SCMR/STS 2017 appropriate use criteria for multimodality imaging in valvular heart disease: a report of the American College of Cardiology Appropriate Use Criteria Task Force, American Association for Thoracic Surgery, American Heart Association, American Society of Echocardiography, American Society of Nuclear Cardiology, Heart Rhythm Society, Society for Cardiovascular Angiography and Interventions, Society of Cardiovascular Computed Tomography, Society for Cardiovascular Magnetic Resonance, and Society of Thoracic Surgeons. Journal of the American College of Cardiology, 2017. 70(13): p. 1647-1672.
5. Zoghbi, W.A., et al., Recommendations for evaluation of the severity of native valvular regurgitation with two-dimensional and Doppler echocardiography. Journal of the American Society of Echocardiography, 2003. 16(7): p. 777-802.
6. Zoghbi, W.A., et al., Recommendations for noninvasive evaluation of native valvular regurgitation: a report from the American Society of Echocardiography developed in collaboration with the Society for Cardiovascular Magnetic Resonance. Journal of the American Society of Echocardiography, 2017. 30(4): p. 303-371.
7. Fidock, B.T., et al., A Systematic Review of 4D-Flow MRI Derived Mitral Regurgitation Quantification Methods. Frontiers in Cardiovascular Medicine, 2019. 6: p. 103.
8. Kamphuis, V.P., et al., Automated cardiac valve tracking for flow quantification with Four-dimensional Flow MRI. Radiology, 2019. 290(1): p. 70-78.
9. Calkoen, E.E., et al., Characterization and quantification of dynamic eccentric regurgitation of the left atrioventricular valve after atrioventricular septal defect correction with 4D Flow cardiovascular magnetic resonance and retrospective valve tracking. Journal of Cardiovascular Magnetic Resonance, 2015. 17(1): p. 18.
10. Roes, S.D., et al., Flow assessment through four heart valves simultaneously using 3-dimensional 3-directional velocity-encoded magnetic resonance imaging with retrospective valve tracking in healthy volunteers and patients with valvular regurgitation. Investigative radiology, 2009. 44(10): p. 669-675.
11. Westenberg, J.J., et al., Mitral valve and tricuspid valve blood flow: accurate quantification with 3D velocity-encoded MR imaging with retrospective valve tracking. Radiology, 2008. 249(3): p. 792-800.
12. Kamphuis, V.P., et al., In-scan and scan–rescan assessment of LV in-and outflow volumes by 4D flow MRI versus 2D planimetry. Journal of Magnetic Resonance Imaging, 2018. 47(2): p. 511-522.

13. She, H.L., et al., Comparative evaluation of flow quantification across the atrioventricular valve in patients with functional Univentricular heart after Fontan's surgery and healthy controls: measurement by 4D flow magnetic resonance imaging and streamline visualization. Congenital heart disease, 2017. 12(1): p. 40-48.
14. van der Hulst, A.E., et al., Tetralogy of fallot: 3D velocity-encoded MR imaging for evaluation of right ventricular valve flow and diastolic function in patients after correction. Radiology, 2010. 256(3): p. 724-734.
15. Westenberg, J.J., et al., Accurate quantitation of regurgitant volume with MRI in patients selected for mitral valve repair. European journal of cardio-thoracic surgery, 2005. 27(3): p. 462-467.
16. Dyverfeldt, P., et al., 4D flow cardiovascular magnetic resonance consensus statement. Journal of Cardiovascular Magnetic Resonance, 2015. 17(1): p. 72.
17. Stout, K.K., et al., Chronic heart failure in congenital heart disease: a scientific statement from the American Heart Association. Circulation, 2016. 133(8): p. 770-801.
18. Crandon, S., et al., Impact of age and diastolic function on novel, 4D flow CMR biomarkers of left ventricular blood flow kinetic energy. Scientific reports, 2018. 8(1): p. 1-11.
19. Töger, J., et al., Hemodynamic forces in the left and right ventricles of the human heart using 4D flow magnetic resonance imaging: Phantom validation, reproducibility, sensitivity to respiratory gating and free analysis software. PloS one, 2018. 13(4).
20. Bock, J., et al., Validation and reproducibility of cardiovascular 4D-flow MRI from two vendors using 2× 2 parallel imaging acceleration in pulsatile flow phantom and in vivo with and without respiratory gating. Acta Radiologica, 2019. 60(3): p. 327-337.
21. Bland, J.M. and D.G. Altman, Statistical methods for assessing agreement between two methods of clinical measurement. lancet, 1986. 1(8476): p. 307-310.
22. Zhong, L., et al., Intracardiac 4D Flow MRI in Congenital Heart Disease: Recommendations on Behalf of the ISMRM Flow & Motion Study Group. Journal of magnetic resonance imaging: JMRI, 2019.
23. Peper, E.S., et al., Highly accelerated 4D flow cardiovascular magnetic resonance using a pseudo-spiral Cartesian acquisition and compressed sensing reconstruction for carotid flow and wall shear stress. Journal of Cardiovascular Magnetic Resonance, 2020. 22(1): p. 1-15.
24. Lai, P., et al. High-Acquisition-Efficiency Cardiac 4D Flow MRI for High-SNR Motion-Robust Imaging with Contrast Agent During Delayed Enhancement Wait Time. in Proc. Intl. Soc. Mag. Reson. Med. 2015.
25. Chelu, R.G., et al., Cloud-processed 4D CMR flow imaging for pulmonary flow quantification. European journal of radiology, 2016. 85(10): p. 1849-1856.

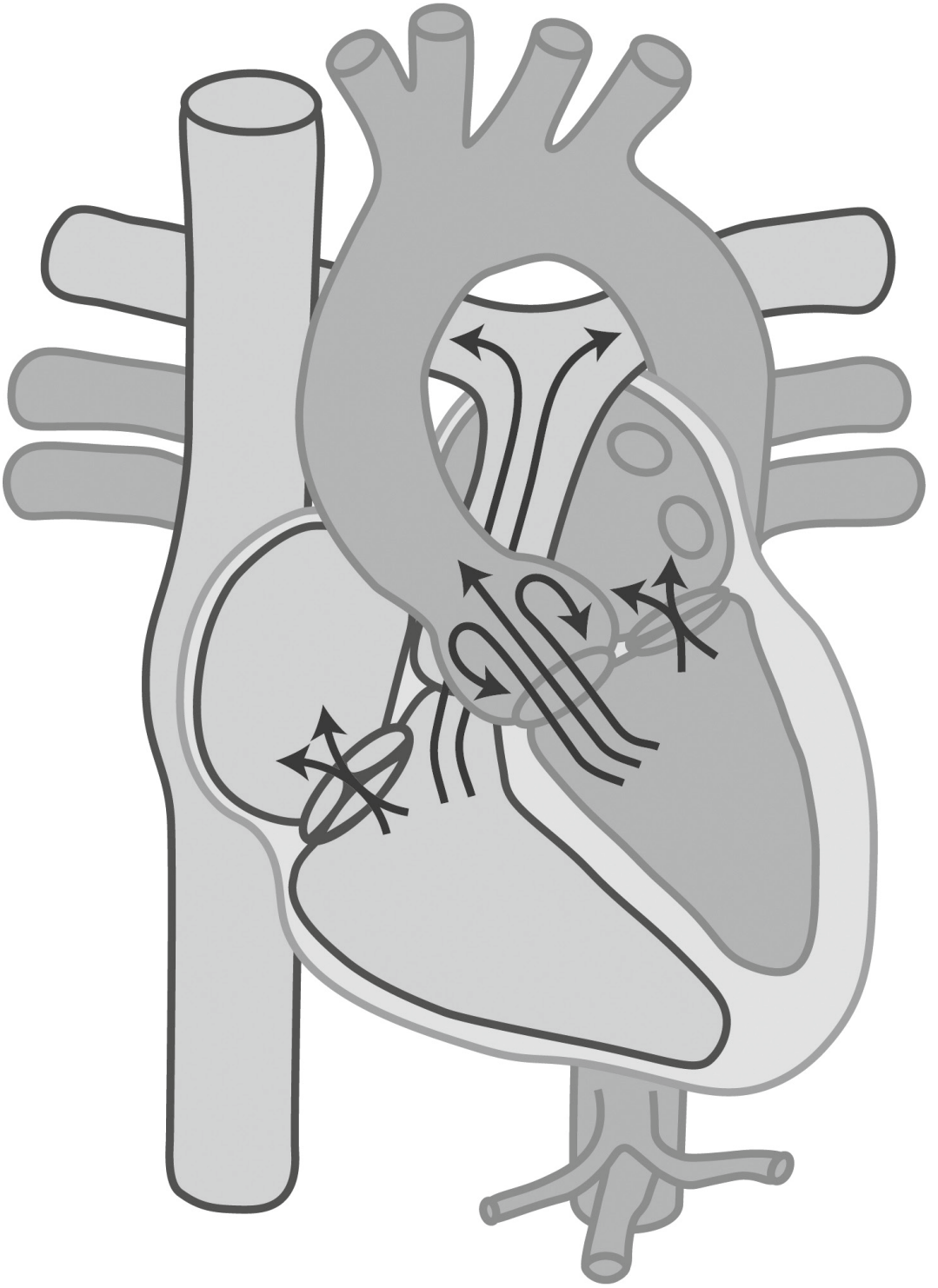

Appendix to Chapter 4

Agreement between 4D flow MRI and echocardiography regurgitation classifications.

The agreement of regurgitation classification between 4D flow MRI and echocardiography was assessed retrospectively for all patients if clinical echocardiography was available. The median absolute time between 4D flow MRI and echocardiography was 2 months (interquartile range 3 months, range 0 – 16 months).

The regurgitation severity was classified based on 4D flow MRI results obtained by the central observer following recommended classification published by the American Society of Echocardiography [5]. For the tricuspid and mitral valve, the regurgitation was classified as none-to-mild (<30%), moderate (30 – 49%) and severe (≥50%). For the pulmonary and aortic valve, the regurgitation was classified as none-to-mild (<20%), moderate (20 – 39%) and severe (≥40%). Echocardiography was performed by various local observers per site (all cardiologists) following international guidelines [5]. To assess the agreement and correlation between 4D flow MRI and echocardiography, a weighted kappa and Spearman's rho correlation coefficients were calculated, respectively. The weighted kappa and Spearman's rho coefficients were classified as: poor (<0.50), moderate (0.50–0.69), good (0.70–0.84), strong (0.85–0.94), and excellent (≥0.95).

Echocardiography was available for 60 patients (60/64, 94%) describing the regurgitation classification of 224 valves (59 tricuspid, 53 pulmonary, 58 mitral, and 54 aortic valves). Over all valves, the statistical analysis demonstrated a good agreement (weighted kappa=0.79, p<0.01) and correlation (r=0.72, p<0.01) between the 4D flow MRI and echocardiography regurgitation classifications, see Appendix Table 1. For the tricuspid, pulmonary, mitral, and aorta valve separately, poor-to-excellent agreements (weighted kappa=0.42, 0.79, 0.65, and 1.00, respectively) and correlations (r=0.50, 0.84, 0.87, and 1.00, respectively) were found, see Appendix Table 2-5.

Appendix Table 1. The echocardiography and 4D flow MRI regurgitation classifications of all valves.

		Echocardiography regurgitation severity			
None-to-mild		None-to-mild	Moderate	Severe	**Total**
4D flow MRI regurgitation severity	None-to-mild	203	3	2	**208**
	Moderate	1	4	4	**9**
	Severe	1	0	6	**7**
	Total	**205**	**7**	**12**	**224**

Appendix Table 2. The echocardiography and 4D flow MRI regurgitation classifications of the tricuspid valve.

		Echocardiography regurgitation severity			
None-to-mild		None-to-mild	Moderate	Severe	**Total**
4D flow MRI regurgitation severity	None-to-mild	55	1	2	**58**
	Moderate	0	0	0	**0**
	Severe	0	0	1	**1**
	Total	**55**	**1**	**2**	**59**

Appendix Table 3. The echocardiography and 4D flow MRI regurgitation classifications of the pulmonary valve.

		Echocardiography regurgitation severity			
None-to-mild		None-to-mild	Moderate	Severe	**Total**
4D flow MRI regurgitation severity	None-to-mild	41	1	0	**42**
	Moderate	1	2	2	**5**
	Severe	1	0	5	**6**
	Total	**43**	**3**	**7**	**53**

Appendix Table 4. The echocardiography and 4D flow MRI regurgitation classifications of the mitral valve.

		Echocardiography regurgitation severity			
None-to-mild		None-to-mild	Moderate	Severe	**Total**
4D flow MRI regurgitation severity	None-to-mild	54	1	0	**55**
	Moderate	0	1	2	**3**
	Severe	0	0	0	**0**
	Total	**54**	**2**	**2**	**58**

Appendix Table 5. The echocardiography and 4D flow MRI regurgitation classifications of the aortic valve.

		Echocardiography regurgitation severity			
None-to-mild		None-to-mild	Moderate	Severe	**Total**
4D flow MRI regurgitation severity	None-to-mild	53	0	0	**53**
	Moderate	0	1	0	**1**
	Severe	0	0	0	**0**
	Total	**53**	**1**	**0**	**54**